metals

MDPI

Article

The Effect of PEO Treatment in a Ta-Rich Electrolyte on the Surface and Corrosion Properties of Low-Carbon Steel for Potential Use as a Biomedical Material

Nádia Marcuz [1], Rafael Parra Ribeiro [2], Elidiane Cipriano Rangel [2], Nilson Cristino da Cruz [2] and Diego Rafael Nespeque Correa [3,*]

[1] FATec—Faculdade de Tecnologia Prof. Wilson Roberto Ribeiro de Camargo, Tatuí 18280-000, SP, Brazil
[2] Laboratory of Technological Plasmas (LaPTec), Science and Technology Institute of Sorocaba (ICTS), São Paulo State University (UNESP), Sorocaba 18087-180, SP, Brazil
[3] Laboratory of Anelasticity and Biomaterials, School of Sciences, São Paulo State University (UNESP), Bauru 17033-360, SP, Brazil
* Correspondence: diego.correa@unesp.br

Abstract: Fe-based materials have extensive applications in the building and automobile industries due to their excellent mechanical properties and low cost. However, their biomedical employment is restricted by the corrosion propensity when in contact with bodily fluids. In this study, single-step Plasma Electrolytic Oxidation, PEO, treatment in Ta-rich electrolyte was used, for the first time, to improve the corrosion resistance of low-carbon steel SAE 1020 for possible use as device implants. The effect of the applied voltage on the chemical and phase composition, topography, wettability, roughness, and corrosion properties were addressed. The results indicated that the Fe-based oxide coatings had a rough and hydrophilic surface, increasing the Ta content with the applied potential. The phase composition of the coatings was mainly composed of hematite (Fe_2O_3), with the Fourier-transform Infrared Spectroscopy, FTIR, spectrums indicating the presence of some absorbed water and organic molecules. The corrosion resistance of the PEO-treated samples was better than the substrate against saline solution (0.9% NaCl) due to the Fe_2O_3 growth decorated with Ta particles, especially the sample treated at 200 V. The results state that Ta-enriched Fe-based oxide coatings could significantly improve the applicability of low-carbon steel SAE 1020 as a low-cost biomaterial, particularly for medical devices.

Keywords: medical devices; low-carbon steel; PEO; Ta; corrosion

Citation: Marcuz, N.; Ribeiro, R.P.; Rangel, E.C.; da Cruz, N.C.; Correa, D.R.N. The Effect of PEO Treatment in a Ta-Rich Electrolyte on the Surface and Corrosion Properties of Low-Carbon Steel for Potential Use as a Biomedical Material. *Metals* **2023**, *13*, 520. https://doi.org/10.3390/met13030520

Academic Editor: Jürgen Eckert

Received: 30 January 2023
Revised: 1 March 2023
Accepted: 2 March 2023
Published: 4 March 2023

1. Introduction

Fe-based materials have wide usage in biomedical applications due to their favorable properties, such as high mechanical strength, good toughness, machinability, and low cost [1]. Their employment as biomedical materials mainly focuses on surgical instruments, medical devices, and healthcare appliances, as well as some specific uses such as hard-tissue replacement and bone-fixation devices for dental [2], orthopedic [3], and cardiovascular [4] systems. Ti and its alloys, Co-Cr alloys, and stainless steel are the most common choices for use as metallic biomaterials [5]. However, the cost still needs to be addressed, limiting their healthcare use in developing countries.

Low-carbon steel SAE 1020 is extensively used in modern society for several components and devices, particularly for building and machine parts, such as rings, axes, columns, and gears [6]. The material combines good mechanical properties, such as elasticity, hardness, wear resistance, and low cost compared to stainless steel. However, Fe is highly reactive with O ions, so the material is very prone to corrosion in an aqueous solution [7]. The corrosion of Fe-based materials (iron and steel) is responsible for considerable financial losses worldwide, which can directly impact the strength and stability of

structures and buildings. Thus, the metallic corrosion of iron requires innovative solutions to overcome this drawback [8]. In this scenery, proper surface modification techniques, which can alter the surface properties without modifying the bulk ones, have been the best choice to improve the corrosion resistance of iron. For example, Yang et al. [9] successfully improved the corrosion resistance of low-carbon steel after plasma electrolytic oxidation (PEO) treatment on an electrolyte enriched with silicate and Al nanoparticles. In contrast, Long et al. [10] obtained reasonable improvements in corrosion resistance after the PEO treatment of Q235 carbon steel in an Al-based electrolyte doped with graphite. Meanwhile, Wang, Jiang, and Yao [11] obtained similar results by forming composite coatings with titania after PEO treatment of carbon steel in a TiO_2-rich electrolyte.

As the surface of iron is bioinert, it does not have a proper interaction with adjacent bone tissues and proteins. Therefore, surface modification by PEO (or MAO—micro-arc oxidation) could be a helpful way to make the surface properties more friendly to the human body [12]. PEO treatment is based on anodic voltage applied to the sample immersed in an electrolyte, and the subsequent dielectric breakdown of the oxide layer, generating plasma discharge generation. As a result, it is possible to grow porous oxide layers firmly bonded to the substrate and enriched with chemical species from the electrolyte [13]. Moreover, this technique has been mainly addressed toward valve metals (e.g., Ti, Al, and Mg), and some papers have successfully reported it in Fe-based materials [9,14–16].

Tantalum (Ta) is a transition metal that is chemically inert at room temperature, possessing excellent corrosion resistance, excellent biocompatibility, and osseointegration ability when in contact with bone tissues. Therefore, pure Ta metal has attracted attention for use in the manufacturing of biomedical implants, despite its high cost [17,18]. Regarding its most stable oxide form (Ta_2O_5), the compound exhibits great biocompatibility, antibacterial ability, superior corrosion, and wear resistance [19,20]. Earlier studies obtained interesting findings depositing a Ta_2O_5 coating after PEO pre-treatment, as an example, by using atomic layer deposition [21], magnetron sputtering [20], and spin coating [22]. However, using PEO, its deposition by a single step could be a cost-effective and innovative strategy to produce Ta_2O_5 biofunctional surfaces.

In the present study, low-carbon steel SAE 1020 samples were submitted to PEO treatment in a Ta-rich electrolyte for the first time. Then, the surface's chemical and phase composition, topography, wettability, and corrosion properties were evaluated in terms of the applied voltages, targeting to pave the way for future use as a medical device.

2. Materials and Methods

2.1. Sample Processing

Rectangular-shaped AISI 1020 carbon steel samples (0.18–0.23 wt% C; 0.30–0.60 wt% Mn; 0.040 wt% P; 0.050 wt% S; Fe balance), with dimensions of $10 \times 5 \times 0.5$ cm^3, were used as substrates. The samples were preliminarily polished with waterproof SiC sandpapers (#220 to #1200) to clean and smooth the surface. Then, the samples were immersed in acetone and washed in an ultrasonic bath for 5 min. PEO treatments were performed in a pulsed power source (MAO-30, Plasma Technology Ltd., Hongkong, China), at voltages of 200, 250, and 300 V, a frequency of 1000 Hz, and a duty cycle of 60%, for 10 min. The electrolyte was composed of an aqueous solution of 2 g·L^{-1} potassium hydroxide (KOH) and 10 g·L^{-1} tantalum hydroxide (TaOH). The electrolyte was previously mixed for 1 h and water-cooled during the PEO treatment. The samples were kept in a dissector until the conducting of the experiments.

2.2. Sample Characterization

The surface morphology of the coatings was examined with Scanning Electron Microscopy (JSM-6010LA, JEOL Ltd., Peabody, MA, USA) using a secondary electron beam (SE) with a spot size of 30 μm at a voltage of 3 kV. Semi-quantitative chemical microanalysis and elemental mapping were performed by X-ray Dispersive Energy Spectroscopy (JEOL Ltd., Peabody, MA, USA), with the detector coupled to the SEM equipment, operating

at 15 kV. In the transmittance mode, the vibrational characteristics of molecular groups absorbed in the surfaces were analyzed using Fourier Transform Infrared Spectroscopy (Jasco Corp., Tokyo, Japan) at room temperature, with 120 scans, resolution of 2 cm^{-1}. The phase composition was evaluated by X-ray Diffraction (XRD; Panalytical X'Pert PRO), with monochromatic CuK_{α} radiation (λ = 0.1544 nm), at a voltage of 40 kV, current of 30 mA, in the continuous scan mode, with a scan speed of 3° per min, and step size of 0.02°. Phase indexation was completed using Highscore Plus® 3.0 software from PANalytical and crystallographic datasheets from the International Centre for Diffraction Data (ICDD). The surface wettability was checked by contact angle measurements (Ramé-hart Instrument Co., Succasunna, NJ, USA) using a droplet of distilled water (30 µL) at room temperature. Arithmetic roughness (Ra) was measured using optical profilometry (Veeco Metrology, Tucson, AZ, USA), with a stylus radius of 12.5 µm, scan length of 2000 µm, resolution of 0.16 µm, during 20 s, and applied load of 3 mgf. Eddy current method (Minipa equipment, model MCT 401) was used to estimate the coatings' thicknesses. The average values were calculated from ten different regions in each sample.

The electrochemical tests were conducted in a three-electrode system, with the sample set up as a working electrode, a platinum wire (Pt) as a counter electrode, and an Ag/AgCl wire as a reference electrode. The electrolyte was composed of an aqueous 0.9% NaCl solution kept at room temperature for all the experiments. The contact area of the sample in contact with the electrolyte was limited by an O-ring (diameter of 1 cm). The open circuit potential (OCP) was measured for 3.6 ks, while the potentiodynamic polarization (PDP) test was measured in the potential range of −1 to 2 V vs. OCP at a scan rate of 1 $mV{\cdot}s^{-1}$ and step of 1 mV. The obtained results were evaluated using NOVA 2.0® software. The corrosion potential (Ecorr), corrosion current density (Icorr), and polarization resistance (Rp) were calculated from Tafel's extrapolation method. The polarization resistance values (Rp) were obtained using the Butler-Volmer equation, and the results were acquired in Tafel's extrapolation (Equations (1) and (2)). I means the current density, η the polarization index, and βa and βc the anodic and cathodic slopes of the Tafel's curves, respectively [23].

$$I = Icorr\left(e^{\left(\frac{\eta}{ba}\right)} - e^{\left(\frac{-\eta}{bc}\right)}\right) \quad (1)$$

$$\frac{1}{Rp} = Icorr\left(\frac{1}{ba} + \frac{1}{bc}\right) \quad (2)$$

3. Results

3.1. Electric Characteristic of the PEO Treatments

Figure 1 shows the current vs. time dependence along the PEO treatment at distinct applied voltages. It can be noted that all samples suffered a sharp decay in the first seconds (step 1: 0–80 s), followed by a moderate one until around 400 s (step 2: 80–400 s), and then a smooth attenuation (step 3: 400–600 s). Step 1 refers to the anodic oxidation reactions of the metallic atoms on the surface to form oxides, while step 2 can be related to the dielectric breakdown of the oxide layer and plasma discharge generation, which affects the current flow through the sample. Then, step 3 is a result of the growth of the thick oxide layer that possesses high electrical resistance, promoting an attenuation of the number of plasma discharges and a gradual reduction of the current. These steps are typical of PEO treatment and were already identified on several valve metals, such as Ti, Al, and Mg [13]. The charge transfer in the samples, calculated from the area under the curve ($Q = \int i.dt$), was around 4.9, 3.7, and 3.6 kC for the 200, 250, and 300 V, respectively. Thus, the increase in the applied potential resulted in a lower charge quantity transferred to the sample, which could indicate a distinct thickness and chemical composition of the oxide layers, as pointed out by Snizhko et al. [24].

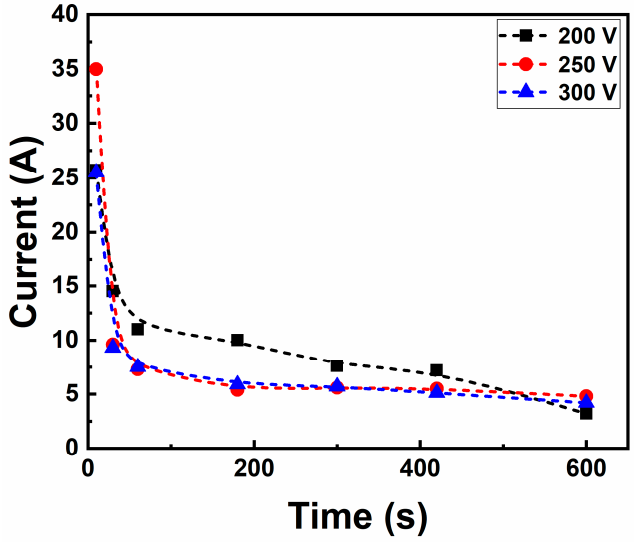

Figure 1. Current vs. time curves of the samples collected during the PEO treatments.

3.2. Topographical Details of the PEO Coatings

The macro and micro topographical aspects of the samples are shown in Figure 2. The optical micrographic image shows that the samples were coated with a brown to gray layer, which was dependent on the applied voltage. At 200 V, the surface seemed brown, changing to gray at 250 V. At 300 V, the sample exhibited a colored aspect and a non-uniform coating. The SEM images displayed rough surfaces with some round pores with a diameter of around 1 µm. The increase in the applied voltage resulted in the appearance of some cavities with a diameter of dozens of micrometers. The dual color of the surface can indicate distinct oxide layers, a thin and dense layer resulting from the anodic and passive oxidative reactions, and a thick and porous one produced during the plasma discharges and species incorporation from the electrolyte. These oxide layers are characteristics of the PEO treatment of metals, having already been identified on Ti [25], Mg [26], and Al [27]. The structures of pores and cavities on the surface result from the plasma discharges that produce channels from the substrate to the outer layer. As a result of high temperature and energy locally in the micro-arcs created during the dielectric breakdown, the plasma discharges remove molten metals from the substrate, which deposit on the surface and are cooled by the electrolyte. The augmenting of the applied voltage increases the energy of the plasma discharges, resulting in a rougher surface and large pores [28]. Thus, it could explain the formation of large cavities on the surfaces of the samples treated at high voltages. In addition, it could be assumed that a dual color aspect on the samples results from the outer oxide layer being removed during the highly energetic plasma discharges.

The EDS elemental mapping of the samples (Figure 3) indicates a plenty distribution of Fe, C, and O atoms on the surfaces, having Fe and C elements originating from the substrate, while O and K come from the electrolyte. The Ta mapping indicated successful incorporation with some agglomerated regions, which could be related to the high temperatures and pressures provided during the plasma discharges. The respective semi-quantitative analysis (Table 1) indicated a majority of Fe and O atoms on the surfaces, evidencing the formation of an oxide layer from the PEO treatment. The amount of Ta remained at a minor concentration, probably enriching the Fe-based oxide layer and gradually increasing with the applied potential. The Ta incorporation can be understood as an effect of the driven force from the applied voltage, which moves the electrolyte's species toward the surface. Similar results were found by Ma et al. [14], who successfully incorporated Si atoms into PEO-treated Q235 low-carbon steel samples. The Si-rich samples exhibited good corrosion resistance for use in the shipping industry.

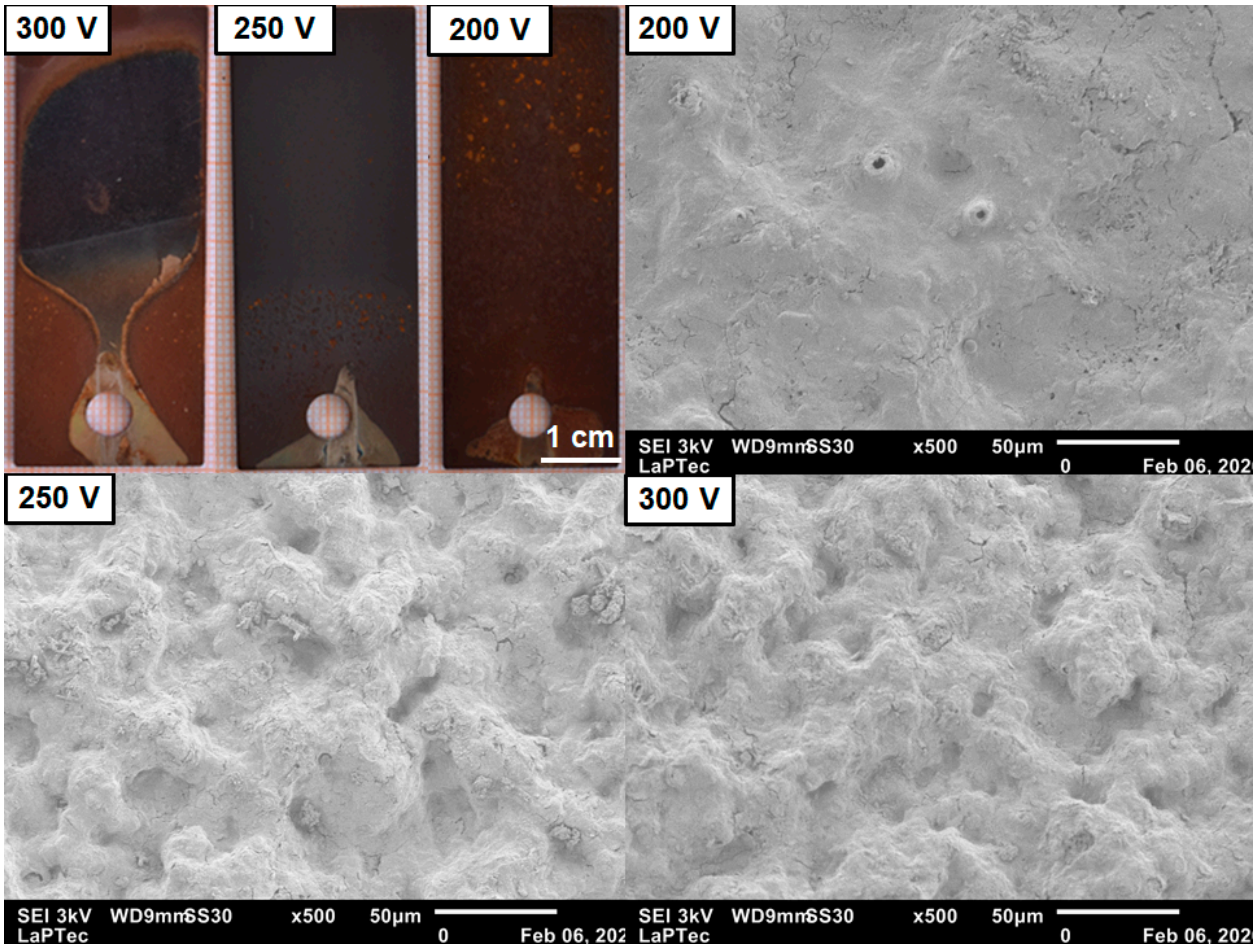

Figure 2. General view and surface topography of the PEO-treated samples.

Table 1. Semi-quantitative EDS chemical analysis (±0.1) of the selected elements on the surface.

(%at.)	Fe	C	O	K	Ta
Substrate	87.6	12.4	-	-	-
200 V	37.6	13.2	46.6	0.6	2.0
250 V	35.2	14.2	46.8	0.8	3.0
300 V	34.6	14.5	46.1	0.9	3.9

3.3. Phase Composition of the PEO Coatings

The phase composition of the substrate and PEO-treated samples are depicted in Figure 4. The non-treated surface exhibited peaks from the BCC crystal structure of Fe, named as ferrite phase (α-Fe, $Im\bar{3}m$). At the same time, some faint diffracted peaks from hematite (Fe_2O_3, $R\bar{3}c$) were noted after PEO treatment. The thick background did not make it possible to distinguish peaks from phases that could be formed during the PEO treatment, such as magnetite (Fe_3O_4, $Fd\bar{3}m$), rust ($Fe(OH)_2$, $P\bar{3}m1$), and Ta_2O_5 (Pmmm), and indicates a low crystallinity of the coatings. In addition, besides the natural tendency of rust formation on the surface of an aqueous solution, the high temperature and pressure resulting from plasma discharges somehow provided the formation of Fe-based oxide instead, which could be advantageous for protection against corrosion [9]. The better corrosion protection of Fe-based oxides has been highlighted in the study of Kim and Kim [29], who performed electrochemical tests in Fe_2O_3, Fe_3O_4, and FeOOH compounds deposited on carbon steel. Ta_2O_5 peaks were not evident in the patterns due to its low concentration in the coatings.

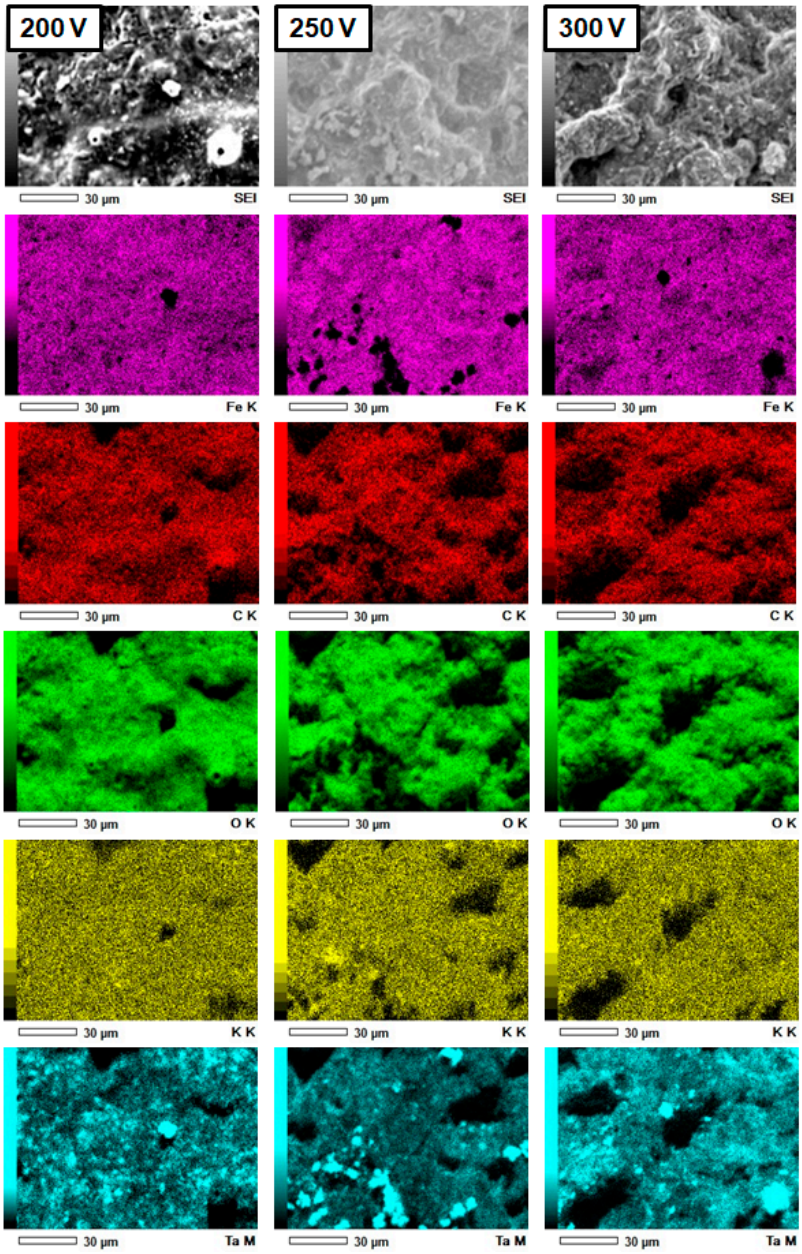

Figure 3. EDS chemical mapping of the elements presented in the samples' surfaces (SEI: Secondary Electron Image; Fe, C, O, and K mappings from the K electron shell; Ta mapping from the M electron shell).

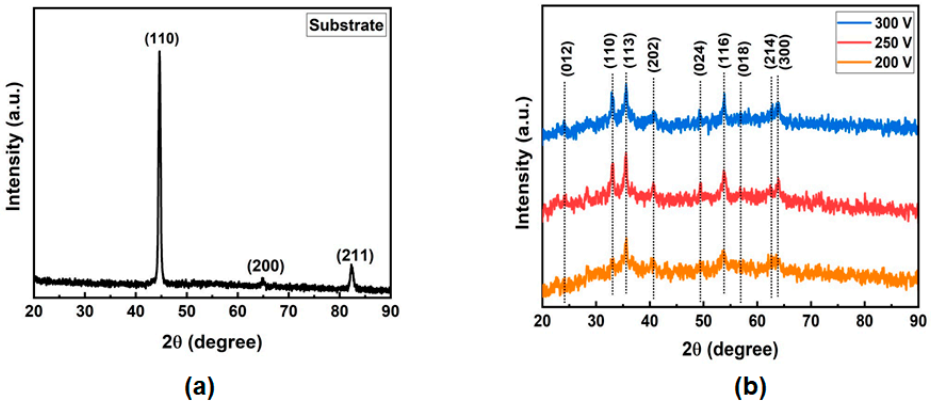

Figure 4. XRD patterns for uncoated substrate (**a**) and PEO-treated samples (**b**).

3.4. Chemical and Physical Aspects of the PEO Coatings

The FTIR spectrums of each sample are shown in Figure 5, where it is possible to identify some bands related to chemical species on the surface. The band around 3290 and 1631 cm^{-1} were identified as stretching (ν) and bending (δ) vibrations of O-H bonding, which was related to H_2O molecules naturally absorbed in the surface [30]. In addition, other bands were also identified in the range of 2000–1000 cm^{-1} related to carbon-based molecules originated from molecules absorbed during PEO treatment and after contact with the atmosphere, e.g., carbon dioxide, alcohols, and organic compounds [31]. A shallow band at around 600–400 cm^{-1} was related to Metal-O bonding, specifically with Fe-O stretching generated by Fe-based oxides (Fe_2O_3 and Fe_3O_4) or hydroxides (FeOOH and $Fe(OH)_2$) [31,32]. It is worth mentioning that it was impossible to identify Ta-O bands in the spectrums due to its low quantity in the coatings and their overlap with the Fe-O bands. For example, Brigth et al. [33] found Ta-O bands from amorphous and nanocrystalline Ta_2O_5 thin films deposited in the Si substrate around 600–200 cm^{-1}.

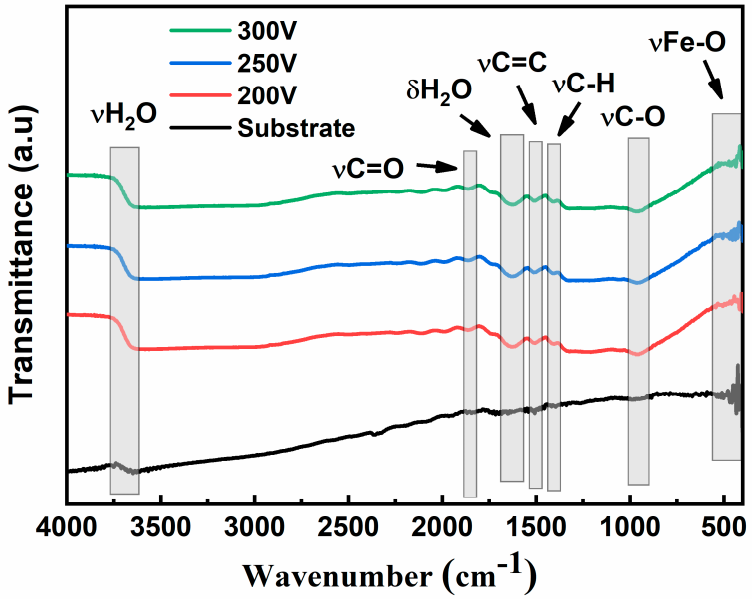

Figure 5. FTIR spectrums with the corresponding vibrational bands indicated in gray rectangles.

Regarding wettability (Figure 6), the substrate depicted a water contact angle that was slightly hydrophilic, while all the PEO-treated samples showed super-hydrophilic surfaces. As it is well known [34,35], low contact angles indicate good adhesiveness and high surface free energy, which favors protein adsorption and cell adhesion, growth, and differentiation. The super-hydrophilic behavior of the surfaces can be directly related to the Ta-enrichment into the oxide layer, which has a high affinity to form hydrogen bonds between hydroxyl molecules and oxygen atoms, as pointed out by Sopata et al. [36].

Some physical characteristics of the PEO coatings are shown in Table 2. The Ra value was smooth for the substrate, while it was rough for the PEO-treated surfaces. The micro-scaled rough surface is a result of the pores and cavities formed during the plasma discharges, having the gradual decay with the applied voltage as a result of the brown outer layer removal detected in Figure 2. As reported earlier, the surface roughness is a crucial issue to consider for biomaterials once it takes a role in regulating the cell behavior at the surface [37]. A micro-sized rough surface enhances cell adhesion and proliferation, collagen synthesis, and mineralization capability compared to nano-sized ones [38]. The average thickness values exhibited a non-linear behavior for the PEO-treated samples, remaining in the order of dozens of micrometers. In addition, the anodic forming rate and the growth constant depicted a significantly difference between the sample treated at 200 V and the others, indicating that low voltage is feasible for producing better PEO

coatings in the sample. The decay of these physical parameters with the applied voltage can be related to the high number of energetic plasma discharges that occurred with the potential rising, which could remove part of the coating [28]. Nie et al. [39] reported that this is a common effect of PEO treatment on non-valve metals, where the thickness growth directly increases the thermal conductivity of the coating, facilitating the plasma discharge. However, thickness in the order of micrometers is enough to adequately protect the bulk against corrosion in the human body [40]. Thus, the results obtained in this study could positively contribute to the potential biomedical applications of the samples.

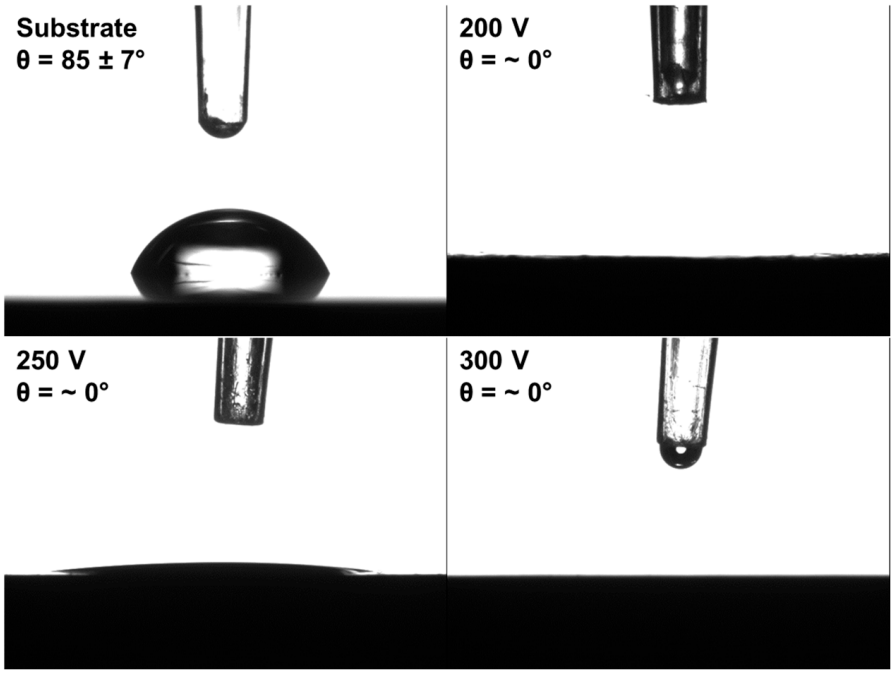

Figure 6. Droplet shapes and contact angles.

Table 2. Physical characteristics of the PEO coatings.

Sample	Ra (μm)	Thickness (μm)	Anodic Forming Rate ($\mu m \cdot s^{-1}$)	Growth Constant ($\mu m \cdot V^{-1}$)
Substrate	1.0 ± 0.1	-	-	-
200 V	7.6 ± 0.2	75 ± 6	0.13	0.38
250 V	3.4 ± 0.3	37 ± 9	0.06	0.15
300 V	2.8 ± 0.5	40 ± 10	0.07	0.13

3.5. Electrochemical Behavior of the PEO Coatings

The samples' corrosion curves and electrochemical parameters are displayed in Figure 7 and Table 3, respectively. The OCP curves (Figure 7a) indicate that the PEO-treated surfaces exhibited more positive values than the substrate, with the sample treated at 200 V having the highest average OCP value. Thus, it can be inferred that the PEO-treated samples have stable surfaces in a 0.9% NaCl solution compared to the substrate. The PDP curves (Figure 7b) also show the better corrosion resistance of the PEO-treated samples compared to the raw material, exhibiting high corrosion potential (Ecorr) and low density current (icorr), although having similar values of polarization resistance (Rp), as depicted in Table 3. Considering that hydrophilic and rough surfaces have deleterious effects on corrosion protection, it can be noted that the better performance of the PEO-treated samples results exclusively from the incorporation of Ta particles. Thus, PEO treatment in a Ta-rich electrolyte could be an exciting strategy to protect low-carbon steel against bodily fluids, particularly saline solution (0.9% NaCl). This result follows some earlier

studies that also addressed the benefits of the PEO treatment on the augmentation of the service life of the material for industrial applications when exposed to distinct corrosive environments [9,15,41].

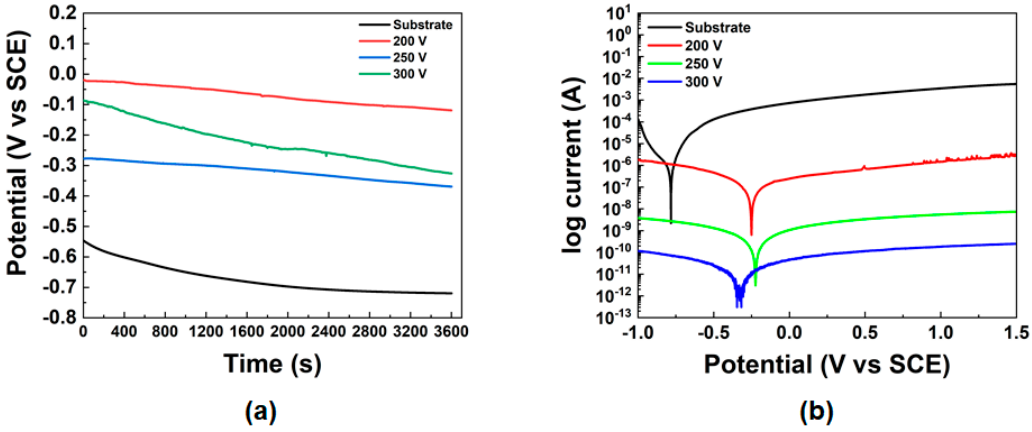

Figure 7. Electrochemical results obtained in 0.9% NaCl solution: OCP (**a**) and PD (**b**) curves.

Table 3. OCP average values and electrochemical Tafel's parameters (±0.01).

Sample	Average OCP (V)	E_{corr} (V)	i_{corr} (nA·cm^{-2})	R_p (MΩ·cm^2)
Substrate	−0.67	−0.79	89.98	6.28
200 V	−0.07	−0.25	3.52	6.32
250 V	−0.32	−0.23	~0.01	5.17
300 V	−0.22	−0.33	~0.01	5.16

For example, Cheng et al. [42] studied the effect of PEO treatment on the corrosion resistance of brass in aluminate electrolyte containing NH_2PO_4 and Na_2SO_3 species using potentiodynamic polarization and electrochemical impedance spectroscopy tests, finding significant improvement of the corrosion resistance, with an efficiency of up to 90%. Meanwhile, Wang et al. [43] produced composite coatings of iron oxides ($FeAl_2O_4$ and Fe_3O_4) using PEO treatment on Q235 steel samples. The OCP measurement in a simulated marine environment (3.5% NaCl solution) indicated initial OCP values of −0.27 V vs. SCE (coated) and −0.66 V vs. SCE (uncoated), which dropped to −0.42 V vs. SCE and −0.69 V vs. SCE, respectively. The corrosion protection of the coated sample was related to the porous and thick oxide layer. Besides the corrosive electrolyte that can penetrate the pores initially, it will reach the inner oxide layer, which is dense and acts as a barrier against corrosive reactions. Thus, the authors concluded that the $FeAl_2O_4$–Fe_3O_4 coating produced by PEO promoted adequate protection of the sample against seawater conditions.

4. Discussion

During the Fe oxidation, redox reactions occur from oxygen and water molecules and the metal. Fe atoms become cations by losing electrons (Equation (3)), while the dissolved oxygen from water forms OH^- radicals following Equation (4). Thus, Fe^{2+} ions bind to OH^- to form iron hydroxide ($Fe(OH)_2$), as indicated by Equation (5). When $Fe(OH)_2$ dries, rust is formed on the surface, which can be easily removed by wear, exposing the metallic surface to the environment and beginning the corrosion process again. The corrosion process is also accelerated in saline solution, due to the presence of dissolved chloride ions ($NaCl \rightarrow Na^+ + Cl^-$). In this environment, the Fe^{2+} ions are balanced by the Cl^- to form ion chlorides ($FeCl_2$) and initiate pitting corrosion points on the metallic surface. As $FeCl_2$ is highly acidic, it contributes to the acceleration of the corrosion process and rust formation [15,43].

$$Fe_{(s)} \rightarrow Fe^{2+}_{(aq)} + 2\,e^- \quad (3)$$

$$O_{2(aq)} + 2H_2O_{(aq)} + 4e^- \rightarrow 4OH^- \quad (4)$$

$$Fe^{2+}_{(aq)} + 2OH^-_{(aq)} \rightarrow Fe(OH)_{2\,(s)} \quad (5)$$

In addition to this, specific features of the environment (e.g., OH^- radicals, temperature, pressure, pH, and chemical composition) can induce the formation of distinct ferrous-based oxides, such as magnetite (Fe_3O_4 or $FeO.Fe_2O_3$), which can be further decomposed to Fe_2O_3 (iron III) or FeO (iron II). Similarly, Fe_2O_3 can be transformed into hematite (α-phase; trigonal crystalline structure) or maghemite (γ-phase; spinel crystalline structure) [14,44]. Interestingly, several reports indicated that hematite could play a positive role in the corrosion resistance of diverse substrates. For example, Tan et al. [45] pointed out that the addition of hematite particles in saturated red soil solutions hindered the corrosion mechanisms of copper, acting as a physical barrier and facilitating the formation of uniform and compact Cu_2O film. Meanwhile, Hoseini, Yarmand, and Kolahi [46] incorporated hematite nanoparticles into TiO_2 film growth by PEO on titanium surfaces. The results indicated a good enhancement of the corrosion properties with 3 $g{\cdot}L^{-1}$ nanoparticles inserted in the PEO solution. The nanoparticles affected the surface reactivity and diminished the ion release in a 3.5% NaCl solution. Furthermore, Ahlström et al. [47] noted the better performance of hematite compared to magnetite when studying the electrochemical properties of steel samples immersed in saturated calcium hydroxide solution with the addition of chlorides.

During the PEO treatment, several plasma discharges occur during the dielectric barrier breakdown of the surface, resulting in local high temperatures and pressures on the oxide layer. This phenomenon competes with the Fe oxidation promoted by the applied voltage, and the plasma discharges more energetically in accord with the applied potential [28,39]. Thus, our results show that plasma discharges originating from the PEO treatment can facilitate the formation of Fe_2O_3 (as hematite) to the detriment of the naturally formed $Fe(OH)_2$, which positively impacts the corrosion behavior of the samples. Nonetheless, as the plasma discharges turn more energetic, they could remove parts of the oxide layer and make the coating non-uniform, as depicted in Figure 2 and noted in the thickness measurements. Thus, the biomedical applicability of the PEO treatment on Fe-based materials should be adjusted for a specific range of voltage to provide a uniform and thick coating on the surface. Finally, the chemical results indicated Ta was successfully incorporated into the Fe_2O_3 coatings during the PEO treatment, which can assist the corrosion protection and favor the biomedical application of low-carbon steel. From the findings, it is possible to draw the scheme indicated in Figure 8, where the effect of applied voltage on the PEO treatment and Ta incorporation on low-carbon steel is expressed.

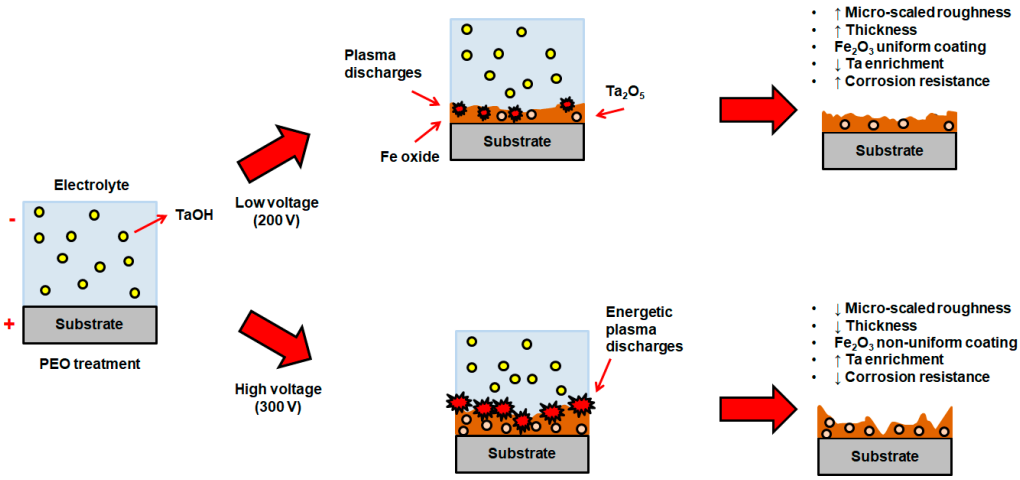

Figure 8. Schematic diagram of the PEO treatment on low-carbon steel substrate based on the results collected at low and high voltages.

5. Conclusions

PEO treatments in a Ta-rich electrolyte were performed on low-carbon SAE 1020 samples at different applied voltages. The findings shows that the biomedical applicability of Fe-based materials can be adjusted by the proper applied voltage in the PEO-treatment, having the Ta incorporation play a role on the corrosion resistance. The morphology exhibited some micro-sized pores and cavities with the voltage rising. The roughness and thickness values remained around 1–8 μm and 30–80 μm, respectively, while the anodic forming rate and growth constant diminished with the applied voltage. FTIR results indicated the presence of absorbed water and carbon-based molecules, with a sharp band around 600–400 cm^{-1} related to the stretching of Fe-O compounds. The Fe_2O_3 oxide was the primary phase in the coatings, having the Ta decorate the surface as a minor component. The PEO-treated surfaces were rougher, hydrophilic, and had improved corrosion properties than the substrate against 0.9% NaCl. Thus, the sample treated at 200 V could be the best option for potential biomedical applications. Further studies focusing on the biological behavior of the PEO-treated samples at 200 V are welcome to evaluate in depth the role of the Ta decoration on the surfaces.

Author Contributions: Methodology, formal analysis, investigation, data curation, and writing—original draft preparation, N.M.; methodology, data curation, and writing—review and editing, R.P.R.; resources, data curation, and writing—review and editing, E.C.R.; resources, supervision, funding acquisition, and writing—review and editing, N.C.d.C.; conceptualization, data curation, supervision, visualization, project administration, and writing—original draft preparation, D.R.N.C. All authors have read and agreed to the published version of the manuscript.

Funding: The authors acknowledge the Brazilian National Council for Scientific and Technological Development (CNPq) grant #407251/2018-9 for the financial support.

Informed Consent Statement: Not applicable.

Data Availability Statement: Data can be shared under request.

Conflicts of Interest: The authors declare no conflict of interest.

References

1. Prasad, K.; Bazaka, O.; Chua, M.; Rochford, M.; Fedrick, L.; Spoor, J.; Symes, R.; Tieppo, M.; Collins, C.; Cao, A.; et al. Metallic Biomaterials: Current Challenges and Opportunities. *Materials* **2017**, *10*, 884. [CrossRef]
2. Tharani Kumar, S.; Prasanna Devi, S.; Krithika, C.; Raghavan, R. Review of Metallic Biomaterials in Dental Applications. *J. Pharm. Bioallied Sci.* **2020**, *12*, S14. [CrossRef]
3. Nasab, M.B.; Hassan, M.R. Metallic Biomaterials of Knee and Hip—A Review. Trends Biomater. *Artif. Organs* **2010**, *24*, 69–82.
4. Jaganathan, S.K.; Supriyanto, E.; Murugesan, S.; Balaji, A.; Asokan, M.K. Biomaterials in Cardiovascular Research: Applications and Clinical Implications. *Biomed. Res. Int.* **2014**, *2014*, 459465. [CrossRef]
5. Sarraf, M.; Rezvani Ghomi, E.; Alipour, S.; Ramakrishna, S.; Liana Sukiman, N. A State-of-the-Art Review of the Fabrication and Characteristics of Titanium and Its Alloys for Biomedical Applications. *Bio-Des. Manuf.* **2022**, *5*, 371–395. [CrossRef]
6. Marulanda Cardona, D.M.; Wongsa-Ngam, J.; Jimenez, H.; Langdon, T.G. Effects on Hardness and Microstructure of AISI 1020 Low-Carbon Steel Processed by High-Pressure Torsion. *J. Mater. Res. Technol.* **2017**, *6*, 355–360. [CrossRef]
7. Martínez, C.; Briones, F.; Villarroel, M.; Vera, R. Effect of Atmospheric Corrosion on the Mechanical Properties of SAE 1020 Structural Steel. *Materials* **2018**, *11*, 591. [CrossRef]
8. Zhang, H.; Liu, D.; Zhao, L.; Wang, J.; Xie, S.; Liu, S.; Lin, P.; Zhang, X.; Chen, C. Review on Corrosion and Corrosion Scale Formation upon Unlined Cast Iron Pipes in Drinking Water Distribution Systems. *J. Environ. Sci.* **2022**, *117*, 173–189. [CrossRef]
9. Yang, W.; Liu, W.; Peng, Z.; Liu, B.; Liang, J. Characterization of Plasma Electrolytic Oxidation Coating on Low Carbon Steel Prepared from Silicate Electrolyte with Al Nanoparticles. *Ceram. Int.* **2017**, *43*, 16851–16858. [CrossRef]
10. Wang, Y.L.; Wang, M.; Zhou, M.; Jiang, Z.H. Characterization of Graphite Containing Ceramic Coating Prepared on Carbon Steel by Plasma Electrolytic Oxidation. *Appl. Mech. Mater.* **2012**, *271–272*, 46–49. [CrossRef]
11. Wang, Y.; Jiang, Z.; Yao, Z. Formation of Titania Composite Coatings on Carbon Steel by Plasma Electrolytic Oxidation. *Appl. Surf. Sci.* **2010**, *256*, 5818–5823. [CrossRef]
12. Lin, Z.; Wang, T.; Yu, X.; Sun, X.; Yang, H. Functionalization Treatment of Micro-Arc Oxidation Coatings on Magnesium Alloys: A Review. *J. Alloys Compd.* **2021**, *879*, 160453. [CrossRef]
13. Clyne, T.W.; Troughton, S.C. A Review of Recent Work on Discharge Characteristics during Plasma Electrolytic Oxidation of Various Metals. *Int. Mater. Rev.* **2019**, *64*, 127–162. [CrossRef]

14. Ma, C.; Liu, J.; Zhu, X.; Xue, W.; Yan, Z.; Cheng, D.; Fu, J.; Ma, S. Anticorrosive Non-Crystalline Coating Prepared by Plasma Electrolytic Oxidation for Ship Low Carbon Steel Pipes. *Sci. Rep.* **2020**, *10*, 15675. [CrossRef] [PubMed]
15. Yang, W.; Li, Q.; Liu, W.; Liang, J.; Peng, Z.; Liu, B. Characterization and Properties of Plasma Electrolytic Oxidation Coating on Low Carbon Steel Fabricated from Aluminate Electrolyte. *Vacuum* **2017**, *144*, 207–216. [CrossRef]
16. Li, H.; Kan, J.; Jiang, B.; Liu, Y.; Liu, Z. Study of the Deburring Process for Low Carbon Steel by Plasma Electrolytic Oxidation. *Plasma Sci. Technol.* **2016**, *18*, 860–864. [CrossRef]
17. Wang, X.; Ning, B.; Pei, X. Tantalum and Its Derivatives in Orthopedic and Dental Implants: Osteogenesis and Antibacterial Properties. *Colloids Surf. B Biointerfaces* **2021**, *208*, 112055. [CrossRef]
18. Han, Q.; Wang, C.; Chen, H.; Zhao, X.; Wang, J. Porous Tantalum and Titanium in Orthopedics: A Review. *ACS Biomater. Sci. Eng.* **2019**, *5*, 5798–5824. [CrossRef]
19. Hu, W.; Xu, J.; Lu, X.; Hu, D.; Tao, H.; Munroe, P.; Xie, Z.-H. Corrosion and Wear Behaviours of a Reactive-Sputter-Deposited Ta 2 O 5 Nanoceramic Coating. *Appl. Surf. Sci.* **2016**, *368*, 177–190. [CrossRef]
20. Huang, H.-L.; Tsai, M.-T.; Chang, Y.-Y.; Lin, Y.-J.; Hsu, J.-T. Fabrication of a Novel Ta(Zn)O Thin Film on Titanium by Magnetron Sputtering and Plasma Electrolytic Oxidation for Cell Biocompatibilities and Antibacterial Applications. *Metals* **2020**, *10*, 649. [CrossRef]
21. Li, C.-Y.; Yu, C.; Zeng, R.-C.; Zhang, B.-C.; Cui, L.-Y.; Wan, J.; Xia, Y. In Vitro Corrosion Resistance of a Ta_2O_5 Nanofilm on MAO Coated Magnesium Alloy AZ31 by Atomic Layer Deposition. *Bioact. Mater.* **2020**, *5*, 34–43. [CrossRef] [PubMed]
22. Zhang, S.; Zou, X.; Liu, N.; Wang, H.; Xia, C.; Liang, C. In Situ Preparation of a Novel Ta_2O_5/MAO Composite Coating on Magnesium for Anti-Corrosion Protection. *Surf. Coat. Technol.* **2022**, *430*, 128003. [CrossRef]
23. Lukács, Z.; Kristóf, T. Determination of Kinetic Parameters from a New Quadratic Approximation of the Butler-Volmer Equation. *J. Electroanal. Chem.* **2022**, *918*, 116443. [CrossRef]
24. Snizhko, L.; Yerokhin, A.; Pilkington, A.; Gurevina, N.; Misnyankin, D.; Leyland, A.; Matthews, A. Anodic Processes in Plasma Electrolytic Oxidation of Aluminium in Alkaline Solutions. *Electrochim. Acta* **2004**, *49*, 2085–2095. [CrossRef]
25. Correa, D.R.N.; Rocha, L.A.; Ribeiro, A.R.; Gemini-Piperni, S.; Archanjo, B.S.; Achete, C.A.; Werckmann, J.; Afonso, C.R.M.; Shimabukuro, M.; Doi, H.; et al. Growth Mechanisms of Ca- and P-Rich MAO Films in Ti-15Zr-XMo Alloys for Osseointegrative Implants. *Surf. Coat. Technol.* **2018**, *344*, 373–382. [CrossRef]
26. Chen, Y.; Dou, J.; Pang, Z.; Yu, H.; Chen, C.; Feng, J. Improving the Corrosion Resistance of Micro-Arc Oxidation Coated Mg–Zn–Ca Alloy. *RSC Adv.* **2020**, *10*, 8244–8254. [CrossRef]
27. Wang, C.; Lu, H.; Yang, H.; Xue, B.; Jia, E.; Chai, G. The Effect of Adding Polyethylene Glycol to Electrolyte Solution on Micro-Arc Oxidation Coating on Pure Aluminum. *Appl. Surf. Sci.* **2022**, *599*, 154047. [CrossRef]
28. Simchen, F.; Sieber, M.; Kopp, A.; Lampke, T. Introduction to Plasma Electrolytic Oxidation—An Overview of the Process and Applications. *Coatings* **2020**, *10*, 628. [CrossRef]
29. Kim, Y.-S.; Kim, J.-G. Corrosion Behavior of Pipeline Carbon Steel under Different Iron Oxide Deposits in the District Heating System. *Metals* **2017**, *7*, 182. [CrossRef]
30. de Alwis, C.; Perrine, K.A. In Situ PM-IRRAS at the Air/Electrolyte/Solid Interface Reveals Oxidation of Iron to Distinct Minerals. *J. Phys. Chem. A* **2020**, *124*, 6735–6744. [CrossRef]
31. Hosseinpour, S.; Johnson, M. Vibrational Spectroscopy in Studies of Atmospheric Corrosion. *Materials* **2017**, *10*, 413. [CrossRef]
32. Raacke, J.; Giza, M.; Grundmeier, G. Combination of FTIR Reflection Absorption Spectroscopy and Work Function Measurement for In-Situ Studies of Plasma Modification of Polymer and Metal Surfaces. *Surf. Coat. Technol.* **2005**, *200*, 280–283. [CrossRef]
33. Bright, T.J.; Watjen, J.I.; Zhang, Z.M.; Muratore, C.; Voevodin, A.A.; Koukis, D.I.; Tanner, D.B.; Arenas, D.J. Infrared Optical Properties of Amorphous and Nanocrystalline Ta_2O_5 Thin Films. *J. Appl. Phys.* **2013**, *114*, 083515. [CrossRef]
34. Kaga, N.; Fujimoto, H.; Morita, S.; Yamaguchi, Y.; Matsuura, T. Contact Angle and Cell Adhesion of Micro/Nano-Structured Poly(Lactic-Co-Glycolic Acid) Membranes for Dental Regenerative Therapy. *Dent. J.* **2021**, *9*, 124. [CrossRef]
35. Al-Azzam, N.; Alazzam, A. Micropatterning of Cells via Adjusting Surface Wettability Using Plasma Treatment and Graphene Oxide Deposition. *PLoS ONE* **2022**, *17*, e0269914. [CrossRef]
36. Sopata, M.; Karpiński, T.M.; Jakubowicz, J.; Sopata, M. Development of Tantalum with Highly Hydrophilic Surface and Antimicrobial Properties Obtained by Micro-arc Oxidation Process. *J. Biomed. Mater. Res. Part B Appl. Biomater.* **2021**, *109*, 829–840. [CrossRef] [PubMed]
37. Cai, S.; Wu, C.; Yang, W.; Liang, W.; Yu, H.; Liu, L. Recent Advance in Surface Modification for Regulating Cell Adhesion and Behaviors. *Nanotechnol. Rev.* **2020**, *9*, 971–989. [CrossRef]
38. Majhy, B.; Priyadarshini, P.; Sen, A.K. Effect of Surface Energy and Roughness on Cell Adhesion and Growth—Facile Surface Modification for Enhanced Cell Culture. *RSC Adv.* **2021**, *11*, 15467–15476. [CrossRef]
39. Nie, X.; Cai, R.; Zhao, C.; Sun, J.; Zhang, J.; Matthews, D.T.A. Advancement of Plasma Electrolytic Oxidation towards Non-Valve Metals. *Surf. Coat. Technol.* **2022**, *442*, 128403. [CrossRef]
40. Correa, D.R.N.; Grandini, C.R.; Rocha, L.A.; Proença, J.P.; Sottovia, L.; Cruz, N.C.; Rangel, E.C.; Hanawa, T. Effect of Temperature on Thermal Oxidation Behavior of Biomedical Ti-Zr-Mo Alloys. *J. Alloys Compd.* **2022**, *905*, 164202. [CrossRef]
41. Yang, W.; Li, Q.; Xiao, Q.; Liang, J. Improvement of Corrosion Protective Performance of Organic Coating on Low Carbon Steel by PEO Pretreatment. *Prog. Org. Coat.* **2015**, *89*, 260–266. [CrossRef]

42. Cheng, Y.; Feng, T.; Lü, J.; Hu, P.; Chen, Y. Plasma Electrolytic Oxidation Behavior and Corrosion Resistance of Brass in Aluminate Electrolyte Containing NaH_2PO_4 or Na_2SiO_3. *Trans. Nonferrous Met. Soc. China* **2022**, *32*, 3985–3997. [CrossRef]
43. Wang, Y.; Jiang, Z.; Yao, Z.; Tang, H. Microstructure and Corrosion Resistance of Ceramic Coating on Carbon Steel Prepared by Plasma Electrolytic Oxidation. *Surf. Coat. Technol.* **2010**, *204*, 1685–1688. [CrossRef]
44. Sangaiya, P.; Jayaprakash, R. A Review on Iron Oxide Nanoparticles and Their Biomedical Applications. *J. Supercond. Nov. Magn.* **2018**, *31*, 3397–3413. [CrossRef]
45. Tan, Y.; Liu, X.; Ma, L.; Li, X.; Liao, Q. The Effect of Hematite on the Corrosion Behavior of Copper in Saturated Red Soil Solutions. *J. Mater. Eng. Perform.* **2020**, *29*, 2324–2334. [CrossRef]
46. Hoseini, A.; Yarmand, B.; Kolahi, A. Inhibitory Effects of Hematite Nanoparticles on Corrosion Protection Function of TiO_2 Coating Prepared by Plasma Electrolytic Oxidation. *Surf. Coat. Technol.* **2021**, *409*, 126938. [CrossRef]
47. Ahlström, J.; Tidblad, J.; Tang, L.; Sederholm, B.; Leijonmarck, S. Electrochemical Properties of Oxide Scale on Steel Exposed in Saturated Calcium Hydroxide Solutions with or without Chlorides. *Int. J. Corros.* **2018**, *2018*, 5623504. [CrossRef]